Hydrogen Bonding on the Ice-Binding Face of a β-Helical Antifreeze Protein Indicated by Amide Proton NMR Chemical Shifts†

Margaret E. Daley,‡ Steffen P. Graether, and Brian D. Sykes*

Department of Biochemistry, CIHR Group in Protein Structure and Function, and Protein Engineering Network of Centres of Excellence, University of Alberta, Edmonton, Alberta T6G 2H7, Canada

Received June 8, 2004; Revised Manuscript Received August 6, 2004

ABSTRACT: The dependence of amide proton chemical shifts on temperature is used as an indication of the hydrogen bonding properties in a protein. The amide proton temperature coefficients of the β-helical antifreeze protein from *Tenebrio molitor* are examined to determine their hydrogen bonding state in solution. The temperature-dependent chemical shift behavior of the amides in *T. molitor* antifreeze protein varies widely throughout the protein backbone; however, very subtle effects of hydrogen bonding can be distinguished using a plot of chemical shift deviation (CSD) versus the backbone amide chemical shift temperature gradient ($\Delta\delta/\Delta T$). We show that differences between the two ranks of ice-binding threonine residues on the surface of the protein indicate that threonine residues in the left-hand rank participate in intrastrand hydrogen bonds that stabilize the flat surface required for optimal ice binding.

The freeze avoidance strategy of many organisms has evolved to include the use of antifreeze proteins to maintain the liquid state of their bodily fluids at temperatures well below the usual minima for their habitat. They do this by keeping their body fluids in a supercooled state, that is, at a point below the equilibrium freezing point, using some interesting adaptations (*1*, *2*). First, contact with potential nucleators is minimized to prevent seeding of ice formation at temperatures at or below the freezing point. Second, many animals produce high levels of sugar alcohols such as glycerol in their body fluids, which depress the freezing point and crystallization temperatures by colligative means. Most interestingly, some organisms also produce antifreeze proteins (AFPs),[1] which specifically bind ice crystals, controlling their growth and preventing them from growing to a size that could cause physical damage.

AFPs have been isolated from various distinct groups of organisms, including fish (*1*), insects (*2*), plants (*3*, *4*), and microorganisms (*5*). The fish AFPs have been classified into five types [antifreeze glycoprotein (AFGP) and AFP types I−IV] based on primary sequence and three-dimensional structural information (*6*). These proteins are all vastly different in primary and tertiary structure, yet all are able to bind to ice and shape its growth. Two types of AFPs unrelated to the fish AFPs have thus far been characterized in detail in insects, one from beetles [*Tenebrio molitor* (Tm) and *Dendroides canadensis*] and the other from the spruce budworm (*Choristoneura fumiferana*). The AFPs from the two insect groups have similar folds (β-helix), but are unrelated at the level of primary sequence and have different coil architectures (*7*−*10*). Despite these differences, the ice-binding surfaces are remarkably similar, consisting of two ranks of precisely aligned threonine residues that appear to match the ice lattice. The insect AFPs have specific activities 10−100 times greater than those of the fish AFPs (*11*). This increased thermal hysteresis activity could be due to the ability of these proteins to bind to two different planes of ice (*8*) or to an increase in the number of ice-binding residues (*12*).

TmAFP is a small (8.4 kDa), highly disulfide-bonded right-handed parallel β-helix consisting of seven tandemly repeated 12-amino acid loops (Figure 1). Both the solution (*9*) and crystal (*7*) structures have been determined and have provided complementary observations. Extensive studies of the backbone and side chain dynamics (*9*, *13*, *14*) using NMR indicate that the entire protein is a very rigid molecule, including the array of threonine residues that comprise the ice-binding face. These data support the emerging hypothesis that it is the intimate surface-to-surface complementarity between the AFP and crystalline ice that is key to the molecular mechanism of antifreeze activity (*15*). The crystal structure provided detailed insight into the unique hydrogen bonding network with external water molecules that mimic a layer of ice (*7*).

The NMR chemical shift of a nucleus has been recognized for many years as a sensitive indicator of molecular conformation, composition, and environment. In proteins, ^{1}H, ^{13}C, and ^{15}N chemical shifts are all used to provide

† This work is supported by grants to B.D.S. from the Canadian Institutes of Health Research (CIHR) and the Protein Engineering Network of Centres of Excellence. M.E.D. acknowledges CIHR for a Doctoral Research Award. S.P.G. is supported by Postdoctoral Fellowships from CIHR and the Alberta Heritage Foundation for Medical Research.

* To whom correspondence should be addressed: Department of Biochemistry, University of Alberta, Edmonton, Alberta, Canada T6G 2H7. Phone: (780) 492-5460. Fax: (780) 492-0886. E-mail: brian.sykes@ualberta.ca.

‡ Present address: Department of Biochemistry and Biomolecular Structure Center, University of Washington, Seattle, WA 98195.

[1] Abbreviations: AFP, antifreeze protein; CSD, chemical shift deviation; $\Delta\delta/\Delta T$, backbone amide chemical shift temperature gradient; HSQC, heteronuclear single-quantum coherence; NMR, nuclear magnetic resonance; TmAFP, *T. molitor* antifreeze protein.

10.1021/bi0488092 CCC: $27.50
Published on Web 09/23/2004

A QCTGGADCTSCT
GACTGCGNCPNA
VTCTNSQHCVKA
NTCTGSTDCNTA
QTCTNSKDCFEA
NTCTDSTNCYKA
TACTNSSGCPGH

B

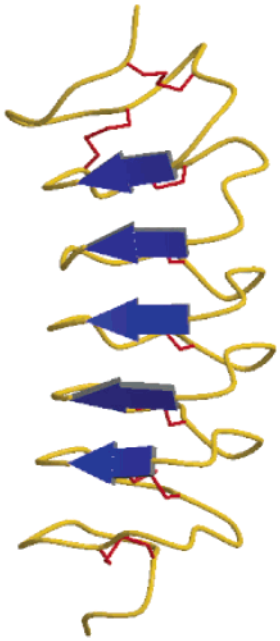

FIGURE 1: Amino acid sequence (A) and NMR structure (B) of the *T. molitor* isoform 2-14 antifreeze protein used in this study. The TmAFP ribbon structure (PDB entry 1L1I) is shown with residues in the parallel β-sheet colored blue and the eight disulfide bonds colored red. This figure was prepared using Molscript (*29*) and Raster3D (*30*).

information about the environment of a particular nucleus, but the complexity of biomolecular systems has made a complete understanding of the basis for protein chemical shifts elusive. Proteins have long been noted to have a wide dispersion of chemical shifts relative to random coil reference data (*16*). In particular, chemical shifts are exquisitely sensitive to the protein secondary structure, and the noted trends are used to deduce preliminary structural information (*17*). Both α-carbons and carbonyl ^{13}C carbons experience a downfield shift when located in α-helices and an upfield shift when in a β-strand or extended conformation, while upfield shifts in α-helical conformations and downfield shifts for nuclei in β-strand and extended conformations are seen for α-^{1}H, amide ^{1}H, and amide ^{15}N chemical shifts. Generally, ^{1}H and ^{13}C chemical shifts are used successfully to determine the most likely secondary structure for a protein sequence using the chemical shift index (CSI) approach (*18*). The relationship between secondary structure and the amide ^{1}H and ^{15}N chemical shifts is typically not exploited for this purpose since they are less well-understood and more factors appear to be involved, making their interpretation more difficult.

The dependence of the chemical shift of amide proton resonances on temperature has been known for many years (*19*). The general trend is that the amide protons experience an upfield shift upon warming, described as a negative temperature coefficient. This effect has been rationalized as a weakening of hydrogen bonding with increased temperature (*20*). In a hydrogen-bonded backbone amide, the carbonyl hydrogen bond partner causes a downfield shift of the amide resonance. With the lengthening of the hydrogen bond caused by an increased temperature, the amide proton is less downfield shifted, resulting in a relative upfield shift. Therefore, solvent-exposed amides will experience a more rapid upfield shift upon warming because of the decrease in intermolecular versus intramolecular hydrogen bonding (*21*). This has led to the widely used practice of attributing temperature gradient ($\Delta\delta/\Delta T$) values less negative than −4 to −4.5 parts per billion/°C (ppb/°C) to the sequestration from solvent of the amide proton. However, this appears to be an oversimplified approach, and other factors, including the chemical shift deviation (CSD) of the resonances from random coil values and the degree of structuring of the protein or peptide of interest (*21*), must be included in the analysis. For example, Baxter and Williamson (*22*) have shown that taking deuterium exchange data into consideration with temperature gradients increases the reliability of determining hydrogen bonding, while Andersen *et al*. (*21*) have demonstrated the utility of correlation plots of NH CSD versus $\Delta\delta/\Delta T$. Although it has been noted that hydrogen-bonded amides in rigid proteins are usually characterized by $\Delta\delta/\Delta T$ values of -2.0 ± 1.4 ppb/°C and exposed amides are more negative, numerous exceptions exist (*21*), and this can only provide a general guideline.

We have applied this analysis to the amide protons of the β-helical TmAFP. We have previously studied the ^{15}N backbone dynamics of TmAFP and have shown that it is a rigid protein that displays restricted internal motions throughout at both 30 and 5 °C (*9*). In the process of assigning the ^{15}N HSQC spectrum at 5 °C for the analysis of ^{15}N relaxation, certain patterns of the temperature gradients and chemical shifts with a decrease in temperature were observed and are studied herein.

EXPERIMENTAL PROCEDURES

The preparation of ^{15}N-labeled TmAFP was previously described (*9*). The sample was prepared for NMR spectroscopy by dissolving the lyophilized protein in a 90% H_2O/10% D_2O mixture containing 0.1 mM DSS (2,2-dimethyl-2-silapentane-5-sulfonic acid). The final protein concentration was approximately 0.4 mM, and the pH of the unbuffered protein was adjusted to 5.5 with microliter aliquots of 100 mM NaOD or DCl as required. It has been previously shown that TmAFP behaves as a monomer in solution and displays no tendency to aggregate under the conditions that have been used (*23*). A series of ^{1}H−^{15}N HSQC spectra for the temperature range of 30−5 °C were collected in 5 °C decrements. The spectra were acquired under identical conditions using a Varian Unity 600 MHz spectrometer equipped with a 5 mm triple-resonance probe and *z*-axis pulsed field gradients. After each temperature change, the sample was allowed to equilibrate for 45 min. Each spectrum was correctly referenced to DSS by collecting a ^{1}H one-dimensional spectrum at each temperature using the same ^{1}H spectral width as for the HSQC spectrum. The spectral width for ^{1}H was 7000.35 Hz and for ^{15}N was 1897.89 Hz;

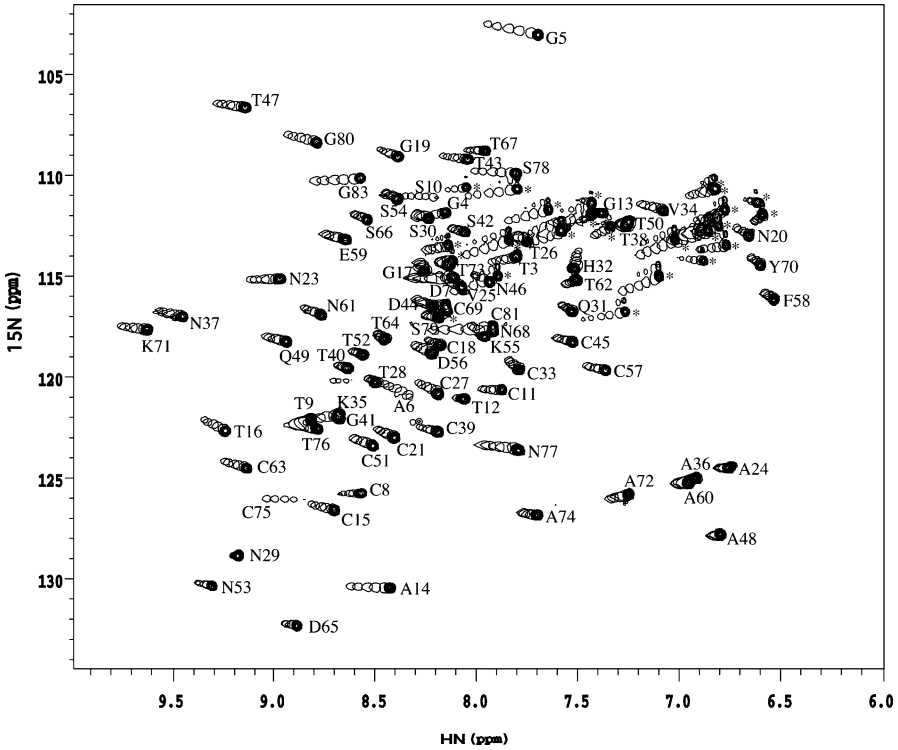

FIGURE 2: Plot of the ^{15}N HSQC spectra displayed as a function of temperature. The 30 °C spectrum is plotted with 10 contours, and the remaining spectra are plotted with one contour at 5 °C intervals down to 5 °C. The amide resonances are labeled with their assignments; those labeled with an asterisk are the Asn and Gln side chain NHs.

436 and 128 complex data points were acquired for ^{1}H and ^{15}N, respectively, with a total of 64 transients collected. The NMR data were processed and displayed using VNMR version 5.3 software on a Sun workstation. The F_2 (^{1}H) dimension was multiplied by a 60°-shifted sine-bell function, and the F_1 dimension was multiplied by a 90°-shifted squared sine-bell function before Fourier transformation.

RESULTS AND DISCUSSION

The ^{15}N HSQC spectra at six temperatures are shown in Figure 2. As the sample is cooled to 5 °C, the amides display the typical downfield shift previously described. Upon closer inspection, it was noted that some residues moved very little or not at all. For example, note T28, T40, T52, and T64 near the middle of the spectrum or N29 in the bottom left corner, which clearly shows no change in chemical shift with temperature. Therefore, we plotted the changes in chemical shift of the individual residues on the TmAFP protein surface (Figure 3) to determine if an overall pattern emerged.

It is immediately obvious that the threonine residues in both ranks on the ice-binding face of the protein experience very little change in chemical shift as the temperature is lowered. The behavior of nearby residues in the protein varies much more widely and may indicate subtle conformational changes that are occurring with changes in temperature. Some residues such as N29 also change little, while others, including A14, T16, and other residues adjacent to the threonine array, do change noticeably. For example, the cysteine residues forming the TCT motif of the ice-binding face have much more negative temperature gradients than the threonines they separate in the sequence.

The temperature gradients (ppb/°C) for each residue are shown in Table 1, which displays both the CSD and $\Delta\delta/\Delta T$ and is sorted by amino acid type. To illustrate the previous result, the temperature gradients for the threonine and cysteine residues in the TCT repeats of the four central loops

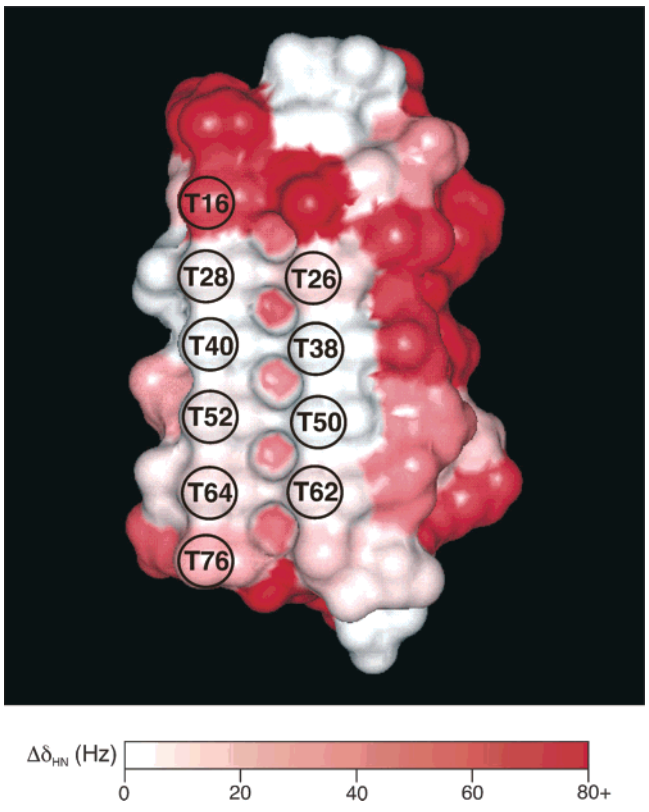

FIGURE 3: Change in amide chemical shifts from 30 to 5 °C mapped on the TmAFP surface (PDB entry 1EZG). The threonine residues on the ice-binding face are labeled. This figure was prepared with InsightII.

Table 1: NH Shift Deviations and Temperature Gradients for TmAFP

residue	NH CSD (ppm)	NH $\Delta\delta/\Delta T$ (ppb/°C)	residue	NH CSD (ppm)	NH $\Delta\delta/\Delta T$ (ppb/°C)
A6	0.07	−4.80	K71	1.38	−4.16
A14	0.24	−6.72	N20	−1.85	−1.52
A24	−1.58	−1.00	N23	0.53	−4.68
A36	−1.41	−1.24	N29	0.63	−0.12
A48	−1.55	−0.68	N37	0.99	−3.88
A60	−1.38	−1.00	N46	−0.56	−2.20
A72	−1.04	−2.76	N53	0.80	−2.28
A74	−0.61	−1.80	N61	0.27	−2.40
C8	0.16	−4.08	N68	−0.36	−10.64
C11	−0.54	−1.68	N77	−0.62	−3.40
C15	0.30	−3.44	Q31	−0.86	−1.08
C18	−0.27	−1.56	Q49	0.59	−2.72
C21	−0.03	−2.56	S10	−0.08	−5.28
C27	−0.23	−3.00	S30	−0.14	−1.40
C33	−0.67	−0.48	S42	−0.31	−1.52
C39	−0.23	−2.84	S54	0.01	−1.40
C45	−0.91	−2.40	S66	0.17	−1.48
C51	0.09	−2.76	S78	−0.42	−8.04
C57	−1.06	−2.68	S79	−0.19	−1.40
C63	0.72	−3.28	T3	−0.60	−4.76
C69	−0.26	−3.04	T9	0.53	0.64
C75	0.52	−7.88	T12	−0.22	−2.76
C81	−0.30	−9.92	T16	1.02	−3.52
D7	−0.27	−6.36	T26	−0.52	−1.24
D44	−0.28	−1.96	T28	0.20	−0.40
D56	−0.27	−2.48	T38	−1.04	−0.20
D65	0.37	−1.40	T40	0.35	−0.60
E59	0.30	−1.72	T43	−0.16	−4.08
F58	−1.84	−0.64	T47	0.95	−4.64
G4	−0.16	−5.12	T50	−1.04	−0.20
G5	−0.51	−8.44	T52	0.28	−0.84
G13	−1.01	−1.68	T62	−0.76	−1.20
G17	−0.18	−0.20	T64	0.16	−0.36
G19	0.02	−2.24	T67	−0.28	−2.68
G41	0.26	−0.40	T73	−0.13	−0.92
G80	0.47	−4.64	T76	0.53	−1.76
G83	0.34	−7.12	V25	−0.07	−3.48
H32	−1.02	1.72	V34	−1.07	−3.16
K35	0.49	−6.24	Y70	−1.65	−1.00
K55	−0.34	−1.32			

were separately averaged. For the left-hand rank of threonines (T28, T40, T52, and T64), the average is −0.55 ppb/°C, and for the right-hand rank of threonines (T26, T38, T50, and T62) it is −0.71 ppb/°C. In contrast, for the cysteines between these threonines (C27, C39, C51, and C63), which form intraloop disulfide bonds, the average was −2.97 ppb/°C. Only C33 has a less negative temperature gradient than the rest of the cysteines in TmAFP; otherwise, the values are remarkably consistent across the disulfide bond pairs. We also observe that the temperature gradient values for the inward-facing alanine and serine residues that line the right and left sides of the protein core, respectively (Figure 4A), cluster in the table and have negative values. The average for the alanines (A24, A36, A48, and A60) is −0.98 ppb/°C and for the serines (S30, S42, S54, and S66) is −1.45 ppb/°C.

Using the general practice of assuming that $\Delta\delta/\Delta T$ values less negative than −4 ppb/°C indicate NH sequestration from solvent would suggest that all of these residues are therefore participating in hydrogen bonds and are protected. However, if the data are plotted in a correlation plot of amide proton CSD versus $\Delta\delta/\Delta T$ (*21*), a very different conclusion is reached. The CSD values are calculated at the lowest temperature of the experiment as $\delta_{obs} - \delta_{ref}$ so that upfield shifts relative to the random coil chemical shift are recorded as negative CSD values. The reference random coil values used are those of Andersen *et al*. (*21*), with the specified correction for temperature of −7.6 ppb/°C (*24*) to adjust the reference values to 5 °C. As devised by Andersen *et al*. (*21*), the plot is formatted with the NH shift deviation on the *x*-axis with downfield NH resonances to the left as in an NMR spectrum. The temperature gradient (*y*) axis is oriented so that amides which experience larger upfield shifts upon warming are at the top of the graph. Figure 4 shows the data for TmAFP plotted in this fashion. In this plot, points appearing toward the lower left represent downfield NHs which do not shift rapidly; these are likely to be intramolecularly hydrogen bonded sites.

The cutoff line at which $\Delta\delta/\Delta T = -2.11 - (\text{CSD} \times 2.41)$ corresponds to that which displays the lowest false positive rate between exchange-protected and exposed amide protons (*21*). With Figure 4A, we re-examine the results for the previously discussed threonine, cysteine, serine, and alanine residues of the central four loops. First is the TCT ice-binding motif, for which there is little change in the chemical shift of the threonines over the 25 °C temperature range that was measured. An interesting observation regarding the CSD for these threonines is noted; although both ranks of threonine have similar values of $\Delta\delta/\Delta T$, they experience different directions in chemical shift relative to the random coil values. The threonines in the left rank (T28, T40, T52, and T64) have an average CSD of 0.25 ppm downfield and are well within the area of the plot corresponding to a high level of potential hydrogen bond formation as marked by the leftmost blue points. However, the threonines in the right-hand rank (T26, T38, T50, and T62) experience an average upfield shift of −0.84 ppm relative to random coil values, putting them on the edge of the designated line and marked as the right-hand blue points, which is a region of the plot where conclusions regarding the hydrogen-bonding state of these residues cannot necessarily be made. This is supported by observation of the hydrogen bonding pattern in the crystal structure using the program VADAR for structural analysis (*25*). In the crystal structure, only the threonine residues in the left-hand rank have their amide protons participating in hydrogen bonds with the carbonyl of the cysteine residue in the strand above. The threonines in the right-hand rank do not make the equivalent hydrogen bonds with their amide proton. This may allow for more rigid placement of the left-rank threonine side chains for interaction with ice. This result is reminiscent of observations made of the two threonine ranks of spruce budworm AFP, where it was proposed that the sequence-conserved right rank bound ice first (*26*).

The cysteine residues between these two ranks of threonine do not appear to be hydrogen bonded; though they have a −2.97 ppb/°C temperature gradient, they also tend to cluster around a CSD value of approximately −0.2 ppm as designated by the red circles. The amides of the serine residues have values quite close to the random coil values; therefore, the CSD is small, and with the −1.45 ppb/°C $\Delta\delta/\Delta T$ value as shown by the light blue triangles in the plot, they also appear to be participating in intramolecular hydrogen bonds. In the TmAFP crystal structure (*7*), the amide protons of the internal serines form intraloop hydrogen bonds to stabilize the tight γ-turns in each loop. The alanine residues, on the other hand, which have an amide $\Delta\delta/\Delta T$

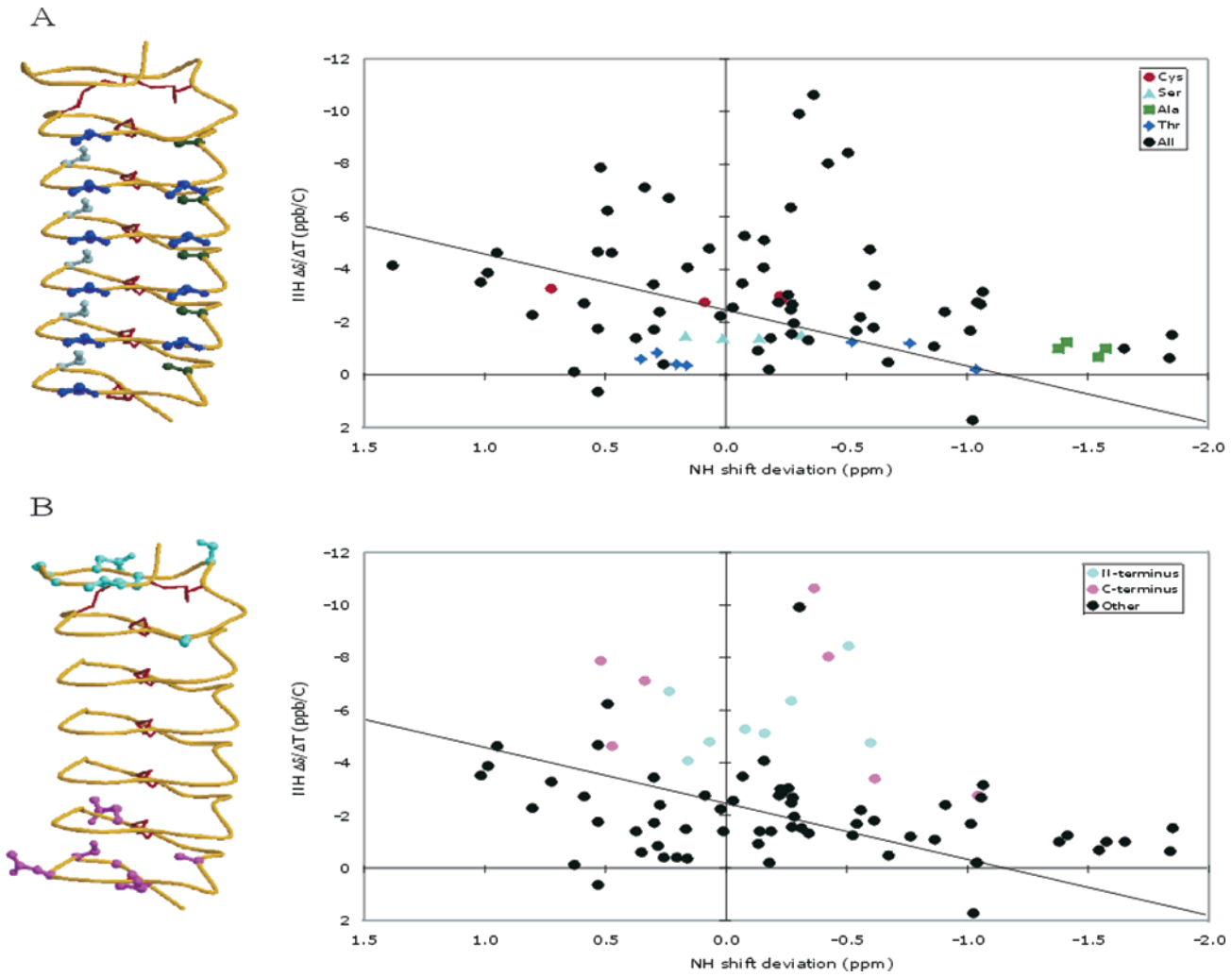

FIGURE 4: Plots of amide CSD vs $\Delta\delta/\Delta T$ for the NHs in TmAFP. The cutoff line corresponds to the relation $\Delta\delta/\Delta T = -2.11 - (\text{CSD} \times 2.41)$ as in ref *21*. The data points are colored as described below and discussed in the text. In panel A, the TmAFP structure (PDB entry 1EZG) is shown with the ice-binding threonines displayed in ball-and-stick representation and colored blue. The eight disulfide bonds are colored red, and the inward-facing serine and alanine residues that line the inside of the coil are also displayed in ball-and-stick representation and colored light blue and green, respectively. Note the change in amino acid residue numbering in this paper relative to the PDB 1EZG coordinates. In this paper, the N-terminal Met used to initiate translation in *E. coli* was numbered 0 to keep the sequence numbering consistent with the native protein (see Figure 1A and ref *9*). In panel B, the N-terminal data points and side chains (T3, G4, G5, A6, D7, C8, S10, and A14) are colored turquoise and the C-terminal residues (N68, A72, C75, N77, S78, G80, and G83) are colored magenta. TmAFP coil figures were prepared using Molscript (*29*) and Raster3D (*30*).

value of −0.98 ppb/°C, are shifted very far upfield, approximately −1.5 ppm from the random coil values and designated by the green squares. This large upfield shift of the alanine residues may be explained by their surrounding environment, which places them in the $i + 3$ position in a constrained β-turn. This position requires very restrictive local backbone dihedral angles and puts the amide proton in the shielding region of the turn amide plane. In this position, the amide proton may be shielded from hydrogen bonding interactions with solvent yet still lack a strong intramolecular hydrogen bond (*27*). Accordingly, from Figure 4A, they appear not to participate in intramolecular hydrogen bonds. A similar observation for a serine with a temperature gradient of approximately −1.5 ppb/°C and a strong upfield shift in a non-hydrogen-bonded amide was made in ubiquitin (*28*). In the crystal structure of TmAFP, the alanine-containing channel also contains five internal water molecules spaced regularly between the loops (*7*). These internal waters form hydrogen bonds to three residues each, including the alanine amide proton. Hydrogen bonding to internal water molecules is likely not as stable as intramolecular hydrogen bonding to other atoms in the protein, since they could be labile, allowing rearrangement of the hydrogen bonding network. This may contribute to the behavior of these alanines in the temperature coefficient and CSD correlation plot.

This is in contrast to the behavior of the terminal residues of TmAFP (Figure 4B) which have CSD values that vary widely and display very negative temperature coefficients. These residues are clearly not participating in hydrogen bonds. Unlike in the core of the protein where both the disulfide bonds and the extensive hydrogen bonding network stabilize the protein, in the termini it appears the disulfide bonds alone are holding the protein intact and some terminal fraying is apparent.

CONCLUSIONS

Overall, a significant portion of the residues in TmAFP appear to be intramolecularly hydrogen bonded. This result

is in agreement with expectations for the parallel β-sheet structure, which contains numerous interstrand hydrogen bonds. Several interesting deviations were noted, particularly at the termini of the protein and for the alanine residues in the protein core. Both the N- and C-termini of the TmAFP lack the hydrogen bonding network involved in stabilizing the rest of the protein. The results for the internal alanine residues may be explained by the unique environment of the alanines in this highly constrained structure as well as by the participation of internal water molecules in the hydrogen bonding network. The chemical shift differences between the two ranks of threonine residues allow for the discrimination of hydrogen bonding properties using the plot of CSD versus $\Delta\delta/\Delta T$. The left-hand rank of threonine residues on the ice-binding face forms intramolecular, interloop hydrogen bonds to help stabilize the flat surface and contributes to the rigidity and surface complementarity required for optimal ice binding.

ACKNOWLEDGMENT

We thank Dr. Peter L. Davies for the ^{15}N-labeled TmAFP used in this study and Gerry McQuaid for his excellent maintenance of the NMR spectrometers.

REFERENCES

1. Fletcher, G. L., Hew, C. L., and Davies, P. L. (2001) Antifreeze proteins of teleost fishes, *Annu. Rev. Physiol. 63*, 359−390.
2. Duman, J. G. (2001) Antifreeze and ice nucleator proteins in terrestrial arthopods, *Annu. Rev. Physiol. 63*, 327−357.
3. Worrall, D., Elias, L., Ashford, D., Smallwood, M., Sidebottom, C., Lillford, P., Telford, J., Holt, C., and Bowles, D. (1998) A carrot leucine-rich-repeat protein that inhibits ice recrystallization, *Science 282*, 115−117.
4. Sidebottom, C., Buckley, S., Pudney, P., Twigg, S., Jarman, C., Holt, C., Telford, J., McArthur, A., Worrall, D., Hubbard, R., and Lillford, P. (2000) Heat-stable antifreeze protein from grass, *Nature 406*, 249−251.
5. Yamashita, Y., Nakamura, N., Omiya, K., Nishikawa, J., Kawahara, H., and Obata, H. (2002) Identification of an antifreeze lipoprotein from *Moraxella* sp. of Antarctic origin, *Biosci., Biotechnol., Biochem. 66*, 239−247.
6. Davies, P. L., and Sykes, B. D. (1997) Antifreeze proteins, *Curr. Opin. Struct. Biol. 7*, 828−834.
7. Liou, Y.-C., Tocilj, A., Davies, P. L., and Jia, Z. (2000) Mimicry of ice structure by surface hydroxyls and water of a β-helix antifreeze protein, *Nature 406*, 322−324.
8. Graether, S. P., Kuiper, M. J., Gagné, S. M., Walker, V. K., Jia, Z., Sykes, B. D., and Davies, P. L. (2000) β-Helix structure and ice-binding properties of a hyperactive antifreeze protein from an insect, *Nature 406*, 325−328.
9. Daley, M. E., Spyracopoulos, L., Jia, Z., Davies, P. L., and Sykes, B. D. (2002) Structure and dynamics of a β-helical antifreeze protein, *Biochemistry 41*, 5515−5525.
10. Leinala, E. K., Davies, P. L., and Jia, Z. (2002) Crystal structure of a β-helical antifreeze protein points to a general ice binding model, *Structure 10*, 619−627.
11. Graham, L. A., Liou, Y.-C., Walker, V. K., and Davies, P. L. (1997) Hyperactive antifreeze protein from beetles, *Nature 388*, 727−728.
12. Leinala, E. K., Davies, P. L., Doucet, D., Tyshenko, M. G., Walker, V. K., and Jia, Z. (2002) A β-helical antifreeze protein isoform with increased activity. Structural and functional insights, *J. Biol. Chem. 277*, 33349−33352.
13. Daley, M. E., and Sykes, B. D. (2003) The role of side chain conformational flexibility in surface recognition by *Tenebrio molitor* antifreeze protein, *Protein Sci. 12*, 1323−1331.
14. Daley, M. E., and Sykes, B. D. (2004) Characterization of threonine side chain dynamics in an antifreeze protein using natural abundance ^{13}C NMR spectroscopy, *J. Biomol. NMR 29*, 139−150.
15. Jia, Z., and Davies, P. L. (2002) Antifreeze proteins: An unusual receptor−ligand interaction, *Trends Biochem. Sci. 27*, 101−106.
16. Wüthrich, K. (1986) *NMR of proteins and nucleic acids*, John Wiley & Sons, New York.
17. Wishart, D. S., Sykes, B. D., and Richards, F. M. (1991) Relationship between nuclear magnetic resonance chemical shift and protein secondary structure, *J. Mol. Biol. 222*, 311−333.
18. Wishart, D. S., and Sykes, B. D. (1994) The ^{13}C Chemical-Shift Index: A simple method for the identification of protein secondary structure using ^{13}C chemical-shift data, *J. Biomol. NMR 4*, 171−180.
19. Ohnishi, M., and Urry, D. W. (1969) Temperature dependence of amide proton chemical shifts: the secondary structures of gramicidin S and valinomycin, *Biochem. Biophys. Res. Commun. 36*, 194−202.
20. Llinás, M., and Klein, M. P. (1975) Charge relay at the peptide bond: a proton magnetic resonance study of solvation effects on the amide electron density distribution, *J. Am. Chem. Soc. 97*, 4731−4737.
21. Andersen, N. H., Neidigh, J. W., Harris, S. M., Lee, G. M., Liu, Z., and Tong, H. (1997) Extracting information from the temperature gradients of polypeptide NH chemical shifts. 1. The importance of conformational averaging, *J. Am. Chem. Soc. 119*, 8547−8561.
22. Baxter, N. J., and Williamson, M. P. (1997) Temperature dependence of ^{1}H chemical shifts in proteins, *J. Biomol. NMR 9*, 359−369.
23. Liou, Y.-C., Daley, M. E., Graham, L. A., Kay, C. M., Walker, V. K., Sykes, B. D., and Davies, P. L. (2000) Folding and structural characterization of highly disulfide-bonded beetle antifreeze protein produced in bacteria, *Protein Expression Purif. 19*, 148−157.
24. Merutka, G., Dyson, H. J., and Wright, P. E. (1995) 'Random coil' ^{1}H chemical shifts obtained as a function of temperature and trifluoroethanol concentration for the peptide series GGXGG, *J. Biomol. NMR 5*, 14−24.
25. Willard, L., Wishart, D. S., and Sykes, B. D. (1997) *VADAR*, version 1.2, University of Alberta, Edmonton, AB.
26. Doucet, D., Tyshenko, M. G., Kuiper, M. J., Graether, S. P., Sykes, B. D., Daugulis, A. J., Davies, P. L., and Walker, V. K. (2000) Structure−function relationships in spruce budworm antifreeze protein revealed by isoform diversity, *Eur. J. Biochem. 267*, 6082−6088.
27. Dyson, H. J., Satterthwait, A. C., Lerner, R. A., and Wright, P. E. (1990) Conformational preferences of synthetic peptides derived from the immunodominant site of the circumsporozoite protein of *Plasmodium falciparum* by ^{1}H NMR, *Biochemistry 29*, 7828−7837.
28. Cierpicki, T., Zhukov, I., Byrd, R. A., and Otlewski, J. (2002) Hydrogen bonds in human ubiquitin reflected in temperature coefficients of amide protons, *J. Magn. Reson. 157*, 178−180.
29. Kraulis, P. J. (1991) Molscript: a program to produce both detailed and schematic plots of protein structures, *J. Appl. Crystallogr. 24*, 946−950.
30. Merritt, E. A., and Bacon, D. J. (1997) Raster3D: Photorealistic molecular graphics, *Methods Enzymol. 277*, 505−524.

BI0488092